Continuous-time quantum-walk spatial search on the Bollobás scale-free network

Tomo Osada,[1,*] Bruno Coutinho,[2] Yasser Omar,[2,3] Kaoru Sanaka,[1] William J. Munro,[4,5] and Kae Nemoto[4]

[1]*Tokyo University of Science, 1-3 Kagurazaka, Shinjuku-ku, Tokyo 162-8601, Japan*

[2]*Instituto de Telecomunicações, Physics of Information and Quantum Technologies Group, Lisbon, Portugal*

[3]*Instituto Superior Técnico, Universidade de Lisboa, Lisbon, Portugal*

[4]*National Institute of Informatics, 2-1-2 Hitotsubashi, Chiyoda-ku, Tokyo 101-8430, Japan*

[5]*NTT Basic Research Laboratories & NTT Research Center for Theoretical Quantum Physics, NTT Corporation, 3-1 Morinosato-Wakamiya, Atsugi, Kanagawa 243-0198, Japan*

(Received 27 August 2019; accepted 6 January 2020; published 10 February 2020)

The scale-free property emerges in various real-world networks and is an essential property that characterizes the dynamics or features of such networks. In this work, we investigate the effect of this scale-free property on a quantum information processing task of finding a marked node in the network, known as the quantum spatial search. We analyze the quantum spatial search algorithm using a continuous-time quantum walk on the Bollobás network, and we evaluate the time T to localize the quantum walker on the marked node starting from an unbiased initial state. Our main finding is that T is determined by the global structure around the marked node, while some local information of the marked node, such as the degree, does not identify T. We discuss this by examining the correlation between T and some centrality measures of the network, and we show that the closeness centrality of the marked node is highly correlated with T. We also characterize the distribution of T by marking different nodes in the network, which displays a multimode log-normal distribution. Especially on the Bollobás network, T is a few orders of magnitude shorter depending on whether the marked node is adjacent to the largest degree hub node. However, as T depends on the property of the marked node, one requires some amount of prior knowledge about such a property of the marked node in order to identify the optimal time to measure the quantum walker and achieve a fast search. These results indicate that the existence of the hub node in the scale-free network plays a crucial role in the quantum spatial search.

DOI: 10.1103/PhysRevA.101.022310

I. INTRODUCTION

Social, technological, or biological systems in the real world often display complex interactions between elements, which cannot be simply explained as regular or random structures. Such real-world systems can be analyzed by mapping their interactions as a graph, often referred to as complex networks. Understanding the structural properties or simulating dynamics in these networks has revealed universal properties of real-world systems [1–3]. Especially, scale-free networks are an important class of networks as they commonly emerge in various systems, such as the World Wide Web, protein interaction in biological organisms, or transport systems such as an airline network [4,5]. Scale-free networks are characterized by their degree distribution following a power-law function of the form

$$\Pi(k) \propto k^{-\beta}, \tag{1}$$

where k is the degree of a node, and the exponent $\beta > 0$ is a real constant (see Fig. 1). Simulating various dynamics on such networks led to a comprehensive understanding of the dynamics in real-world systems such as the fast spreading of information [6–9].

On the other hand, a recent development in engineering quantum systems has enabled us to design complex quantum systems that are beyond regular lattice structures [10–13]. Analyzing quantum dynamics or performing a quantum-information processing task on such complex quantum networks is becoming of great interest, and it is important to examine what difference or improvement we can see from these systems compared to regular lattice systems [14–17].

Toward that end, we analyze here a quantum-information processing task to find a marked node in a graph, which is known as the spatial search, on a scale-free network. Searching a marked item in a database is one of the most fundamental and important computational problems. The spatial search is the case in which each item of the database is represented as each node of a network, and one aims to find a marked node using some quantum dynamics and measurement defined in the network [18–20]. One can achieve this by using the framework presented by Childs and Goldstone [20], which prepares a black box Hamiltonian that encodes the network adjacency matrix and the information of the marked node, and performing a continuous-time quantum walk using that Hamiltonian. Since the network structure is encoded in the Hamiltonian, we can observe how the scale-free property of the network will affect the quantum walk and the spatial search.

Under the framework of the continuous-time quantum walk, the spatial search has been extensively studied on

*tosada92@gmail.com

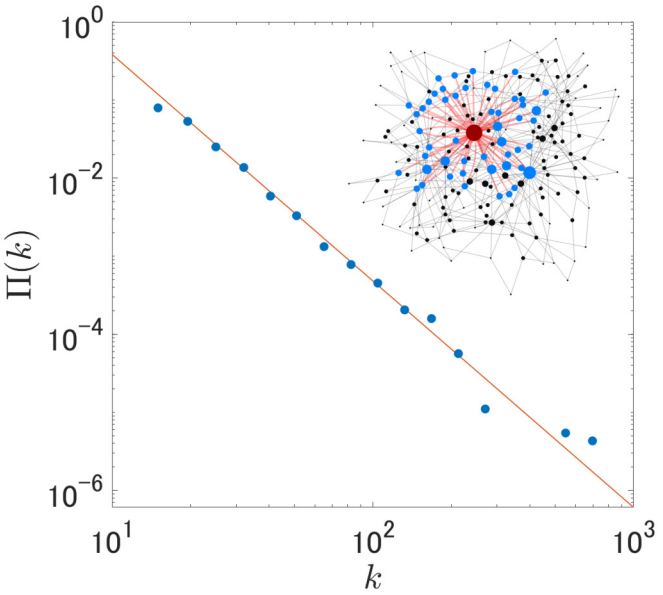

FIG. 1. Degree distribution of the Bollobás model with network parameters $N = 10\,000$, $m = 5$, $\beta = 2.9$. The red solid line is the fitting curve of the blue data points acquired from the generated network. Inset: visualization of the network for $N = 200$, $m = 2$, $\beta = 3$. The size of the nodes is determined by the closeness centrality of its node, the red node placed at the center of the network has the largest degree (the hub node) with its edges drawn as red bold lines, and the blue nodes connected to them are the neighbors of the hub node.

various graphs. Much work has been done considering regular graphs or lattice structures [20–24], as well as a comprehensive analysis of the spatial search using Erdös-Rényi random graphs [25] or general Markov chains [26]. The main focus of these studies was on whether one can achieve the search with the time complexity of $O(\sqrt{N})$ on the given graph. Some work moved toward exploring nonregular structures. Agliari *et al.* [27] explored a spatial search on fractal structures and studied how the transition in the ground state of the Hamiltonian depends on the marked node. Berry and Wang [28] studied a spatial search with a discrete-time quantum walk on a Cayley tree, and they examined the relation between the search and centrality measures of the graph. Philipp *et al.* [29] examined balanced trees, and they observed that the search performance changes depending on whether the marked node is toward the root or the leaves of the graph. Although each of these studies provided important results to characterize some correlation between the graph structure and the spatial search, we still do not know how the spatial search will behave in complex networks.

To further clarify our aim, we point out two differences that we expect between the complex networks in which we are interested, and the handful of graphs mentioned above. First, the nodes in a complex network are mostly nonequivalent to each other. A counterexample is the nodes in lattices with a periodic boundary condition, which are all equivalent due to the translational symmetry. Secondly, complex networks are not purely random, and some order lives in the randomness. A typical example is the scale-free network, as they have hub nodes that have a substantially larger degree than the others, while most nodes have a small degree. To satisfy these conditions, we choose the Bollobás model [30,31], a mathematical model to generate the scale-free network obeying preferential attachment [4], as the network in which to analyze the spatial search.

Searching nodes on scale-free networks using classical random walks has been investigated in the literature in terms of analyzing the hitting time or the mean first-passage time [32–34]. In the Barabási-Albert network, the mean first-passage time is shown to be roughly proportional to the degree of the target node [32]. Regarding the dependency on the network size N, the mean first-passage time scales linearly to N [33], while sublinear scaling was also found in special cases such as searching the hub node [34]. In our work, we will also discuss how the quantum nature leads to different results compared to the above classical cases.

Through our numerical simulations, first we will show that the speed of the spatial search using the quantum walk indeed depends on which node in the network is marked, due to the nonequivalence of the nodes. Surprisingly, this speed can be different by up to a few orders of magnitude. This is the first critical difference compared to searching on regular or lattice graphs. We characterize how this dependency emerges in terms of the leading eigenvector (the eigenvector corresponding to the largest eigenvalue) of the network adjacency matrix. This reveals that the performance of the algorithm is dominated by the localized property of the leading eigenvector. To further characterize the relation between the network structure and the performance of the search, we examine the correlation between some centrality measures of the network and the time complexity of the quantum search. We find that the degree and the time complexity of the search are not strongly correlated, unlike the search using a classical random walk. The speed is determined instead by the shortest path distances between the marked node and the rest of the nodes. This observation cannot be seen from purely random graphs [25], and this is another critical difference from the previous studies. We also point out one advantage of using a scale-free network for the spatial search, which is that one can perform the search starting from a localized initial state instead of a global superposition state conventionally used in the spatial search. From this, one can naturally translate the spatial search to an efficient state transfer protocol between the hub node and another arbitrary node. All of these results indicate that the hub node plays an important role in the spatial search algorithm.

II. MODELS

Let us begin by defining the spatial search algorithm we are going to examine. Defining $G(V, E)$ as a graph (such as shown in Fig. 1, inset) with a set of nodes $V = \{1, 2, \ldots, i, \ldots, N\}$ and a set of edges E, we consider an N-dimensional Hilbert space spanned by the basis states $\{|1\rangle, |2\rangle, \ldots, |i\rangle, \ldots, |N\rangle\}$. Each state corresponds to the situation in which a quantum walker is localized at node i. We can then define the state of the quantum walker at time t as $|\psi(t)\rangle = \sum_{i=1}^{N} c_i|i\rangle$ with c_i constrained such that $\sum_{i=1}^{N} |c_i|^2 = 1$. To search for a single marked node (labeled $|w\rangle$ in this case), we let the state

$|\psi(t=0)\rangle$ evolve under the action of the Hamiltonian

$$H = -\gamma A - \epsilon_w |w\rangle\langle w| \tag{2}$$

$$= -\gamma \sum_{i,j}^{N} A_{ij}(|i\rangle\langle j| + |j\rangle\langle i|) - \epsilon_w |w\rangle\langle w|, \tag{3}$$

where A is the adjacency matrix of graph $G(V, E)$ whose entries are defined as $A_{ij} = A_{ji} = 1$ if nodes i and j are connected by an edge, and otherwise $A_{ij} = 0$. The real constant $\gamma \geqslant 0$ is the transition energy between the nodes, and ϵ_w is the on-site energy on node w. The projection $|w\rangle\langle w|$ causes the amplitude to accumulate on the marked node w. We consider the unitary time evolution of the system given by

$$i\hbar \frac{d}{dt}|\psi(t)\rangle = H|\psi(t)\rangle, \tag{4}$$

and we compute the probability to measure the quantum walker at the marked node $P(t) = |\langle w| \exp(-iHt/\hbar)|\psi(0)\rangle|^2$. The time complexity of the algorithm or the "search time" T, in units of $\hbar/\epsilon_w$, is evaluated by finding the shortest time $t = \tau$ that maximizes $P(t)$. As one can find the quantum walker on node w with probability $P(\tau)$ at the optimal measurement time τ, the algorithm can identify the marked node with success probability $P(\tau)$. We finally compute $T = \tau/P(\tau)$, which takes into account the repetition of the algorithm for $1/P(\tau)$ times.

Although we are aware that the Hamiltonian in Eq. (3) has limitations when the underlying graph is nonregular [35], and a modified search Hamiltonian has been proposed [25], we use the Childs and Goldstone formalism since our interest is focused on investigating how the quantum dynamics is affected when the Hamiltonian itself has a scale-free property. Modifying the Hamiltonian based on the method by Chakraborty *et al.* [25] will be advantageous to analyze the time complexity on arbitrary graphs systematically, but it also compensates for the inhomogeneity of the graph. This will compensate for the scale-free property of the underlying graph, which conflicts with the purpose of this paper. Additionally, the search Hamiltonian by Childs and Goldstone could be experimentally realized on quantum simulators [36] without requiring gate decomposition of the algorithm on quantum computers. For these reasons, in our work we keep our focus on the Hamiltonian formalized by Childs and Goldstone.

Next we describe how the preferential attachment (PA) model is generated, and we point out some properties of this network. We use the formalization by Bollobás [30,31]. The process of generating the network with N nodes is as follows: At the initial time step $u = 1$, the network $G_{\{u=1\}}$ starts with a single node v'_1 with one edge connecting to itself. At every subsequent time step $u \geqslant 2$, one node v'_u having one outgoing edge is added to $G_{\{u-1\}}$ and connects to one of the nodes in $G_{\{u\}}$ with its outgoing edge. Defining the degree of node v'_i at time u as $d_u(v'_i)$, the node to connect to is chosen by the following probability distribution [30]:

$$\Pr(i = s) = \begin{cases} d_{u-1}(v'_s)/(2u-1), & 1 \leqslant s \leqslant u-1, \\ 1/(2u-1), & s = u. \end{cases} \tag{5}$$

This means that the probability for a node to be chosen is proportional to its degree, which resembles the "preferential attachment." After repeating the above process until a certain time step $u = m$ ($m \in \mathbb{N}$), the set of nodes $v'_1, v'_2, \ldots, v'_m$ forms a single node v_1. The edges that were connecting the nodes within the set are converted to m self-loops on v_1. The process of adding new nodes v'_u is continued until a time step $u = 2m$, and again the set of nodes $v'_{m+1}, \ldots, v'_{2m}$ forms another node v_2. If $m' \leqslant m$ nodes in the set of nodes $v'_{m+1}, \ldots, v'_{2m}$ are connected to v_1, they are converted to m' edges between v_1 and v_2. Following the rule described above, the process is repeated until time step $u_{\text{end}} = mN$, which results as a network $G_{\{mN\}}$ with N nodes and mN edges. The obtained network has a power-law degree distribution with exponent $\beta = 3$ [30]. To change the value of β, we use the method introduced by Dorogovtsev *et al.* [37].

From the construction above, we have three control parameters when generating the network; the total number of nodes N, the parameter that controls the connectivity of the network m, and the degree distribution exponent β. The average degree of the network is $2m$, while the minimum degree is m and the largest degree is $\sim N^{1/(\beta-1)}$. Note that we allow self-loops and parallel edges between nodes in our network in order to maintain consistency, that is, to fix the total number of edges to mN for every trial of generating $G_{\{mN\}}$. When converting $G_{\{mN\}}$ to the adjacency matrix A, the number of self-loops or parallel edges contributes to the weight of the diagonal or the off-diagonal entries of A, respectively. The degree distribution and visualization of an instance of $G_{\{mN\}}$ are shown in Fig. 1.

Although there are many other scale-free network models proposed in the literature [38–42], in this paper we focus only on this Bollobás model to make our problem more tractable. The Bollobás model has no high clustering coefficient, community structure, or a self-similar structure. We leave the examination of the effect of such properties on the spatial search for future work, and we take advantage of the simplicity of Bollobás model to concentrate on how the power-law degree distribution affects the spatial search.

III. SEARCH TIME ON THE BOLLOBÁS MODEL

As the first step to analyzing the search time on the Bollobás model, we consider an abstract dynamics of the spatial search algorithm to show that the search time will depend on the selection of the target node in the network. We define two states $|\lambda_1\rangle$ and $|\tilde{w}\rangle$ as

$$|\lambda_1\rangle = (|E_0\rangle - |E_1\rangle)/\sqrt{2}, \tag{6}$$

$$|\tilde{w}\rangle = (|E_0\rangle + |E_1\rangle)/\sqrt{2}, \tag{7}$$

where $|E_{0,1}\rangle$ are the lowest and second lowest energy eigenstates of our Hamiltonian H, with the parameter γ chosen at a specific value $\gamma = \gamma_{\text{opt}}$. We assume that the two lowest energies are nondegenerate. We also assume that $|\lambda_1\rangle$ is the leading eigenvector of A, such that $A|\lambda_1\rangle = \lambda_1|\lambda_1\rangle$. This assumption of Eqs. (6) and (7) is based on degenerate perturbation theory [20], and it can also be confirmed from Fig. 3. Next, we are going to consider the unitary evolution where the initial state is $|\lambda_1\rangle$, which will rotate to $|\tilde{w}\rangle$ in time $\pi/\Delta E$. Here $\Delta E \equiv E_1 - E_0$ is the gap between the energies corresponding to the eigenstates $|E_{0,1}\rangle$. It is straightforward to show that

$$\Delta E = 2|\langle\lambda_1|w\rangle\langle w|\tilde{w}\rangle|. \tag{8}$$

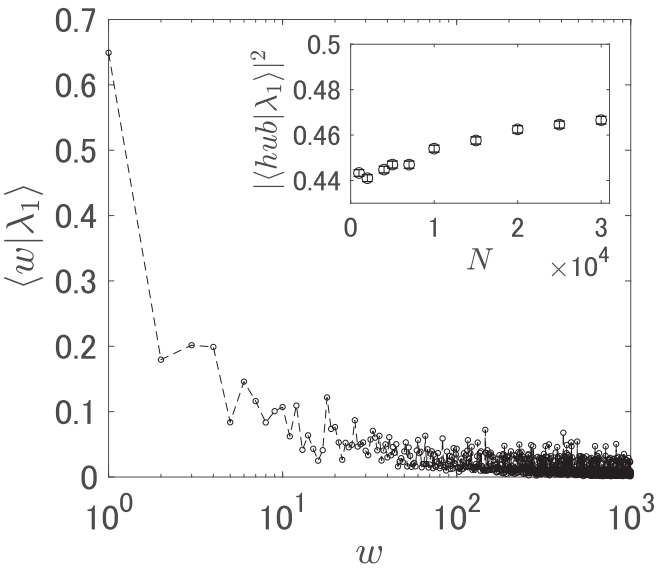

FIG. 2. Plot of the overlap $\langle w|\lambda_1\rangle$ vs w, showing all components of the leading eigenvector (the eigenvector corresponding to the largest eigenvalue of the network adjacency matrix) from one instance of our Bollobás model with network parameters $N = 1000$, $m = 10$, $\beta = 3$. The eigenvector, all components of which are real and positive, displays a localized property around the large degree nodes. Index $w = 1$ is the largest degree hub node. Inset: The squared component on the largest degree node $|\langle \text{hub}|\lambda_1\rangle|^2$ for different sizes of the Bollobás model with $m = 10$ and $\beta = 3$. Since there is a substantial overlap between $|\text{hub}\rangle$ and $|\lambda_1\rangle$, and the value does not decrease when N is increased, we can select the state $|\text{hub}\rangle$ as the initial state without degrading the scaling of the search time.

The first factor in Eq. (8) tells us that the energy gap (and equivalently the evolution time $\tau = \pi/\Delta E$) depends on the component c_w of the leading eigenvector $|\lambda_1\rangle = \sum_{i=1}^{N} c_i|i\rangle$. One has $\langle\lambda_1|w\rangle = 1/\sqrt{N}$ for any index w if the adjacency matrix A is the one for regular graphs or if the Laplacian matrix is used. However, for nonregular graphs the components of the leading eigenvector are not uniform. As in the preferential attachment network, it was shown by Goh *et al.* [43] that the components of $|\lambda_1\rangle$ are localized on the largest-degree node, and c_i varies from $1/\sqrt{2}$ to $1/(2\sqrt{N})$. Figure 2 confirms this property of $|\lambda_1\rangle$ for the network we have generated. The value of the second factor in Eq. (8) is nontrivial, since we need to know $\langle w|E_0\rangle$ and $\langle w|E_1\rangle$, but in principle this also depends on the index w if the graph is nonregular. It is worth mentioning that $|\langle w|\tilde{w}\rangle|^2$ represents the success probability P, and thus P and τ are related through $\langle\lambda_1|w\rangle$.

As the second step of the analysis, we discuss the optimization of γ in Eq. (3) and the selection of the initial state $|\psi(0)\rangle$. The parameter γ has to be chosen at an optimal value γ_{opt} so that the search will work in the most efficient way. Specifically, γ_{opt} is chosen to be the value for which Eq. (6) is approximately true. In our numerical simulation, γ_{opt} is determined by finding the point where $|\langle\lambda_1|E_0\rangle|^2 \approx |\langle\lambda_1|E_1\rangle|^2 \approx 0.5$ is achieved. This point is shown graphically in Fig. 3. In addition to γ, the initial state of the time evolution $|\psi(0)\rangle$ has to be chosen properly for the search to work. Clearly

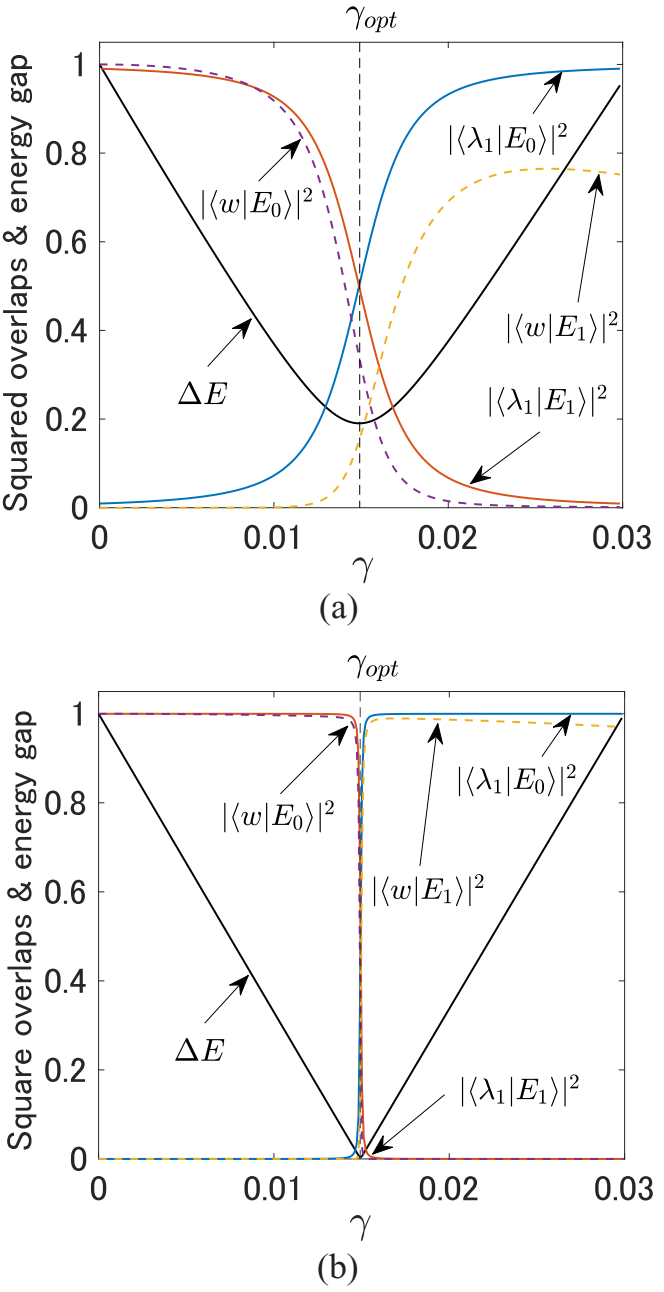

FIG. 3. Plots of the squared overlaps of the states of interest, and the energy gap $\Delta E \equiv E_1 - E_0$ of the Hamiltonian H. The Bollobás model with $N = 2000$, $m = 10$, $\beta = 3$ is used in this plot. By changing the value of γ (plotted in units of ϵ_w), we can see the quantities $|\langle\lambda_1|E_{0,1}\rangle|^2$ change from 0 to 1 and vice versa, which confirms that the eigenstates $|E_{0,1}\rangle$ switch around $\gamma = \gamma_{\text{opt}}$. This also confirms that $|\lambda_1\rangle = (|E_0\rangle - |E_1\rangle)/\sqrt{2}$ is approximately achieved at $\gamma = \gamma_{\text{opt}}$. ΔE is minimized at this point. The quantities $|\langle w|E_{0,1}\rangle|^2$ are shown to indicate how close the resulting state of the time evolution $|\tilde{w}\rangle$ is to $|w\rangle$. Part (a) represents the case when a node with a large degree is marked, and (b) represents the case when a node with the smallest degree in the network is marked. Part (a) has the larger ΔE at $\gamma = \gamma_{\text{opt}}$ compared to (b), which indicates that the evolution time τ is smaller. One can also see that the switch of eigenstates around $\gamma = \gamma_{\text{opt}}$ is much sharper in (b).

the ideal choice is $|\lambda_1\rangle$, since we want the dynamics to stay inside the two-dimensional subspace spanned by $|E_{0,1}\rangle$. On the other hand, the search still works (it shows a high success probability) using a state that has a substantial overlap with $|\lambda_1\rangle$. Here, we utilize the localized property of $|\lambda_1\rangle$ (see the inset of Fig. 2), and we choose an initial state where the quantum walker is fully localized at the single largest-degree hub node. We define this state as $|\text{hub}\rangle$ for convenience. On the other hand, we have confirmed that the uniform superposition state over all nodes $\sum_{i=1}^{N}|i\rangle/\sqrt{N}$, which is conventionally used in the spatial search, has a small overlap with $|\lambda_1\rangle$. For all of the following results, our simulation is performed with $|\psi(0)\rangle = |\text{hub}\rangle$.

Now let us describe the simulation results, where we have numerically computed the maximum probability to measure the quantum walker after evolving for an optimal time τ, $P(t=\tau) = |\langle w|\exp(-iH\tau/\hbar)|\psi(0)\rangle|^2$. As we know that τ and $P(\tau)$ depend on the index of the marked node w, we will take full account of which node in the network was marked when evaluating the search. To this end, we first show the distribution of the search time $T = \tau/P(\tau)$. We get the distribution by generating multiple samples of the Bollobás model with a fixed $\{N, m, \beta\}$, repetitively marking a random node for each network, finding γ_{opt} and computing T, and finally taking the histogram of T. We have excluded the largest-degree hub node when randomly marking a node, since we initialize the quantum walker on that site. Figure 4 shows the distribution for three different values of $\beta = 2.5, 3, 3.5$, with fixed N and m. Note that the distribution is taken in logarithmic scale. The main feature in this distribution is that they have multiple peaks, meaning that there are classes of nodes that can be searched faster or slower than each other. A good fit to the distributions was a sum of log-normal functions in the form

$$f(T) = \sum_i p_i g(T;\mu_i,\sigma_i), \tag{9}$$

where

$$g(T;\mu,\sigma) = \frac{1}{\sqrt{2\pi}\sigma T}\exp\left(\frac{(\ln T-\mu)^2}{2\sigma^2}\right). \tag{10}$$

Therefore, the distribution $f(T)$ is characterized by the mean values μ_i, standard deviations σ_i, and the mixing parameters p_i (constrained such that $\sum_i p_i = 1$). For the distributions with $\beta = 2.5$ and 3 we take up to $i = 4$, and for $\beta = 3.5$ we take up to $i = 3$.

We understand that this multimode log-normal distribution results from the randomness of the network and the effect of the hub node. When we take a distribution of the search time on the Erdös-Rényi random graph, we see a single-mode log-normal distribution. Likewise, the connections of the nodes in the Bollobás model are mostly random (meaning that there are no characteristic structures such as communities or self-similarity) except that the overall degree distribution follows a power law. However, this power-law degree distribution, or the large-degree hub node, heavily influences the nodes around it, leading to the multimode distribution. In fact, we find that the narrower modes μ_3 and μ_4 (and μ_2 for $\beta = 2.5$) correspond to the nodes that are directly connected to the largest-degree hub. We will discuss this further in Sec. IV.

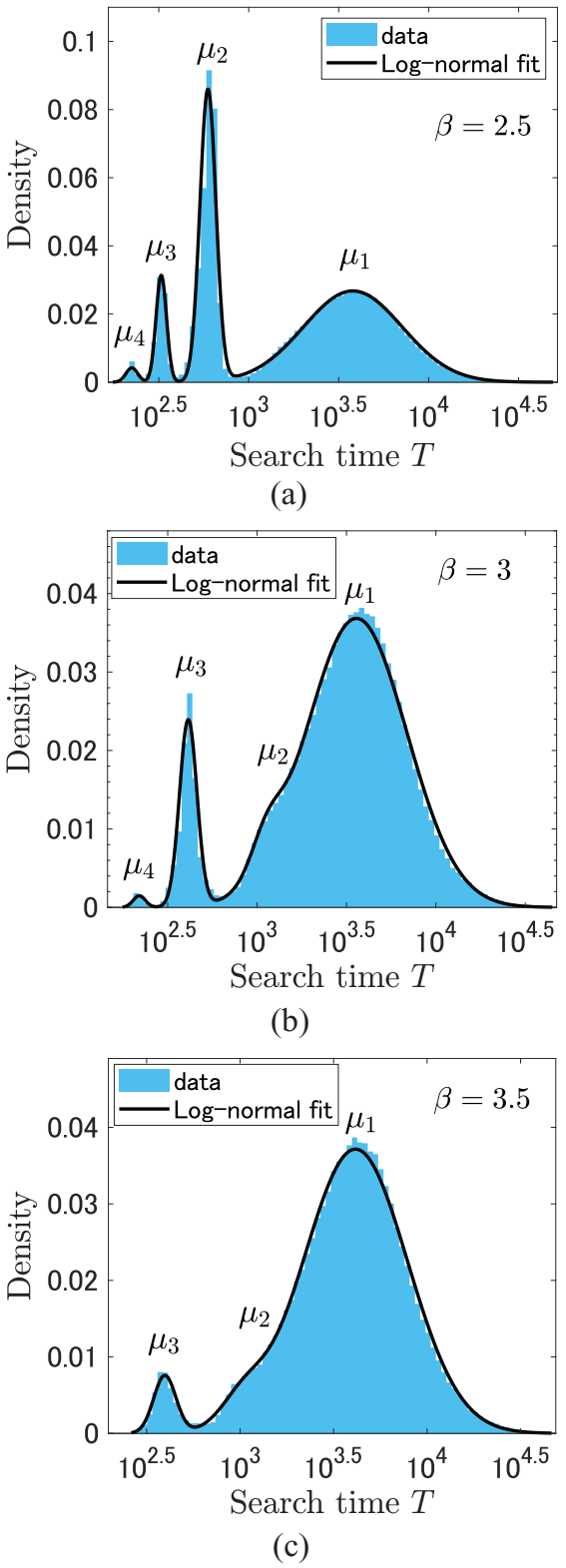

FIG. 4. Distributions of the search time T, in a logarithmic scale, for networks with $N = 10\,000$, $m = 10$ and (a) $\beta = 2.5$, (b) $\beta = 3$, and (c) $\beta = 3.5$, respectively. To obtain each distribution, we have generated 1000 network samples and computed T for at least 400 randomly selected nodes from each network sample. For all distributions we observe multiple peaks, and we find that they are best fit to a sum of log-normal distributions. The symbols $\mu_1, \ldots, \mu_4$ indicate the individual modes.

TABLE I. Exponent α of each parameter of the search time distribution fit to $\propto N^{\alpha}$. Obtained from networks with $N = 2000$–$10\,000$, $m = 10$, and $\beta = 2.5, 3, 3.5$. "const" indicates that the quantity is independent of N.

	$\beta = 2.5$	$\beta = 3$	$\beta = 3.5$
μ_1	0.731 ± 0.021	0.620 ± 0.024	0.681 ± 0.032
μ_2	0.295 ± 0.010	0.254 ± 0.040	0.256 ± 0.027
μ_3	0.253 ± 0.009	0.194 ± 0.014	0.172 ± 0.014
μ_4	0.240 ± 0.006	0.155 ± 0.012	N/A
σ_1	0.147 ± 0.026	0.180 ± 0.032	0.155 ± 0.029
σ_2	-0.013 ± 0.005	-0.133 ± 0.035	const
σ_3	const	-0.016 ± 0.004	const
σ_4	const	const	N/A
p_1	0.213 ± 0.018	0.211 ± 0.022	0.112 ± 0.030
p_2	-0.132 ± 0.034	-1.65 ± 0.54	-0.942 ± 0.096
p_3	-0.478 ± 0.043	-0.423 ± 0.061	-0.613 ± 0.057
p_4	-0.847 ± 0.055	-0.920 ± 0.086	N/A

Next we evaluate the scaling of the parameters μ_i, σ_i, p_i by examining their dependence on N, specifically by fitting to the function $\propto N^{\alpha}$. The obtained scaling exponents α are shown in Table I, and the plots of μ_i versus N are shown in Fig. 5. We find two features in our results. First, for all β, μ_1 has $\alpha > 0.5$ while $\mu_{i\geqslant 2}$ has $\alpha < 0.5$. As $\alpha = 0.5$ is the best known scaling of the spatial search algorithm, the scaling of $\mu_{i\geqslant 2}$ being $\alpha < 0.5$ has to be interpreted carefully, and we are not claiming here that a spatial search faster than $T \propto N^{0.5}$ can be achieved. The search time evaluated here is the case when the measurement of the quantum walker is done at the exact optimal time τ when the probability $P(\tau)$ maximizes. To know the optimal time, one must first know the properties of the marked node, or at least know that the node is in one of the modes of $\mu_{i\geqslant 2}$ in order to make a reasonable guess of the measurement time. Therefore, our result does not mean that a search faster than $N^{0.5}$ can be achieved for some nodes in the network, but rather that the quantum walker can be localized to those nodes quickly. Additionally, by identifying the number of nodes $\tilde{N}$ that is involved in the modes $\mu_{i\geqslant 2}$, and by fitting to $\tilde{N}^{\alpha}$, the scaling reduces to $\alpha \approx 0.5$.

The second feature in our result is the agreement between the scaling of p_i and the property of the network. From Table I, we see that $p_{i\geqslant 2}$ decays as N grows. This corresponds to the decay of the fraction of nodes that are neighbors of the largest hub node, $N^{1/(\beta-1)}/N$. The result suggests that the modes $\mu_{i\geqslant 2}$ correspond to the nodes that are neighboring to the hub, or the nodes heavily influenced by the hub. This argument is also supported by the change of the distributions depending on β (see Fig. 4). As β increases, edges will be less concentrated on the large-degree nodes, allowing the network to become closer to a random graph. This effect is observed as the shrinking of the $\mu_{i\geqslant 2}$ modes when β increases. We note that these scalings obtained from numerical simulations are only guaranteed for $N = 2000$–$10\,000$, the region where we executed the simulations.

As a conclusion of this section, the distribution of the search time T obtained by marking different nodes in the network strictly reflects the structure of the network; the randomness and scale-free property (i.e., existence of the hub) lead to a multimode log-normal distribution of T. The existence of the hub allows the quantum walker to localize especially quickly on the nodes that are the neighbors of the hub.

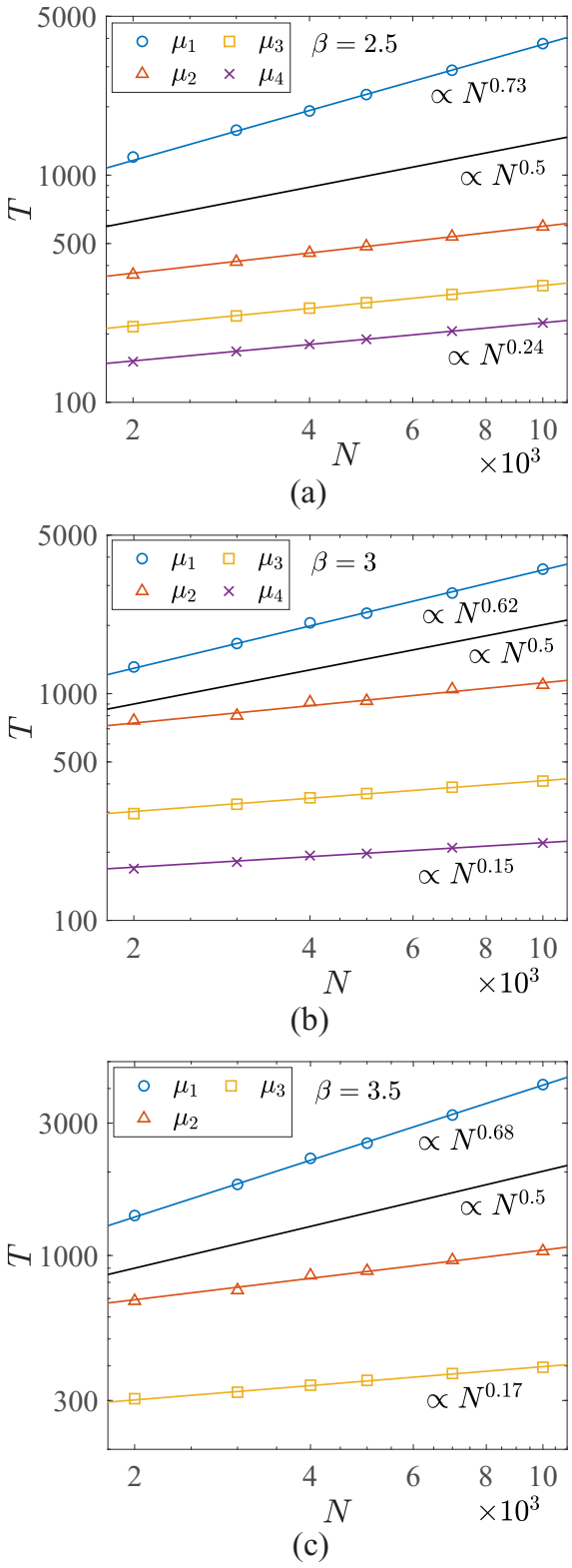

FIG. 5. Dependence on the network size N of the average values of the search time distribution $\mu_1, \ldots, \mu_4$ for networks with $m = 10$ and (a) $\beta = 2.5$, (b) $\beta = 3$, and (c) $\beta = 3.5$, respectively. The black solid line of $N^{0.5}$ is drawn as a reference.

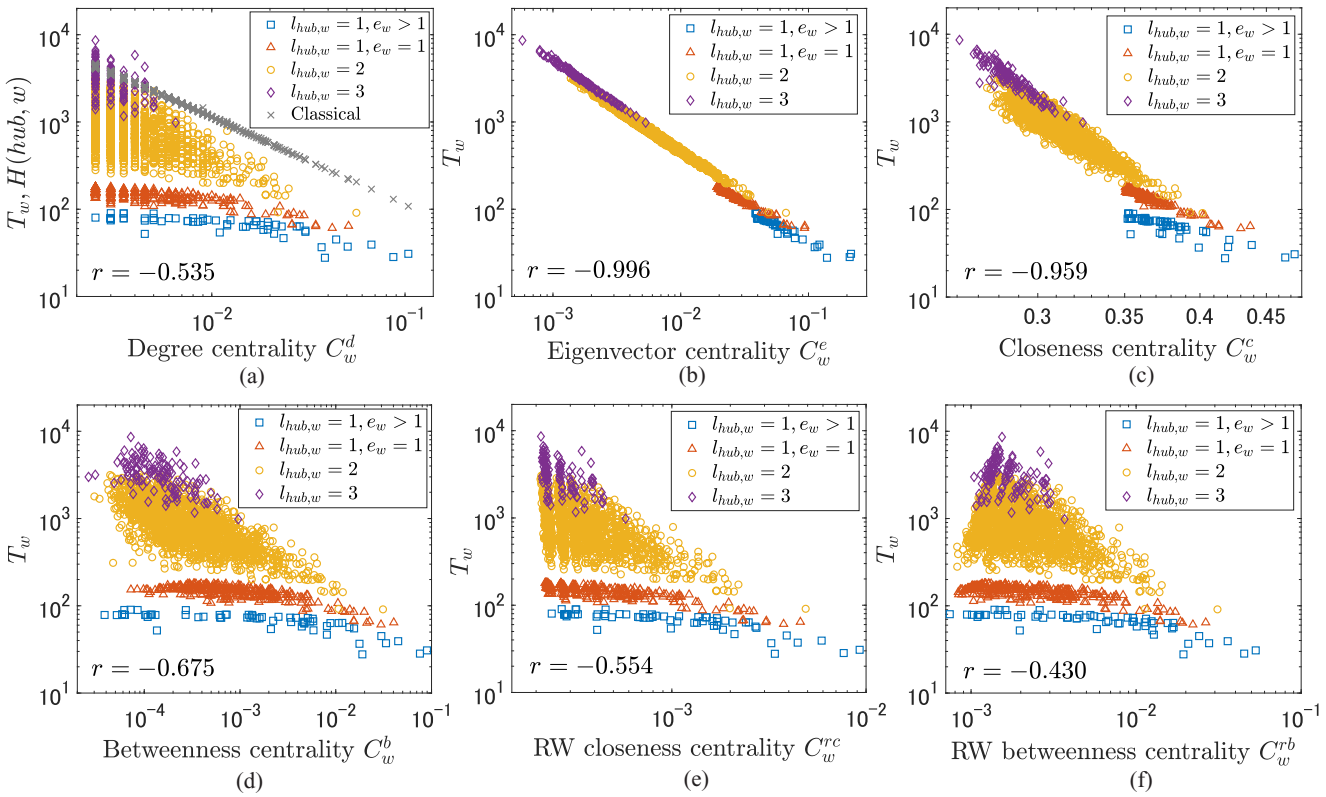

FIG. 6. The correlation between the search time T and six different network centrality measures, which are (a) degree centrality, (b) eigenvector centrality, (c) closeness centrality, (d) betweenness centrality, (e) RW closeness centrality, and (f) RW betweenness centrality. All of the scatter plots are in log-log scale, and each data point corresponds to each node of the network with parameters $N = 2000$, $m = 5$, $\beta = 3$. Data points have different symbols depending on the shortest path distance between the largest degree hub node and the marked node $l_{\mathrm{hub},w}$, as well as depending on whether the marked node has parallel edges to the hub or not for $l_{\mathrm{hub},w} = 1$. e_w in the legend represents the number of parallel edges between the hub and the marked node (or equivalently the weight $A_{\mathrm{hub},w}$). In (a), the mean first-passage time of the classical random walk $H(\mathrm{hub}, w)$ (a walk from the hub to the marked node w) is also plotted. The best correlation between the centrality measures and the quantum search time is seen from (b) eigenvector centrality, followed by (c) closeness centrality. The Pearson correlation coefficient r of the centrality measures and the search time (both in logarithmic scale) is shown inside the figures.

IV. CHARACTERIZATION OF THE SEARCH THROUGH NETWORK CENTRALITY MEASURES

In this section, we interpret the search time T and the dynamics of the spatial search by investigating some centrality measures of the network. This will bridge the knowledge in complex network science and quantum dynamics. We investigate the correlation between the search time and six different centrality measures: degree centrality, eigenvector centrality [44], closeness centrality [45], betweenness centrality [46], random-walk closeness centrality [47], and random-walk betweenness centrality [48]. The essential result we show here is that the search time is dependent on how close the marked node is to all other nodes in the network, in terms of the shortest path distances.

The scatter plots where the search time T is plotted against different centrality measures are shown in Fig. 6. Figure 6(a) shows the case of degree centrality $C_w^d = \sum_j^N A_{wj}/(N-1)$, which measures the fraction of nodes that are connected to the node w. This plot shows that when the marked node has a large degree, the quantum walker will likely be localized on that node quickly, but if the node has a low degree, the search time is almost independent of the degree. This feature is quite different from the case of the classical random walk, where the difference can be seen by comparing with the mean first-passage time $H(\mathrm{hub}, w)$ computed numerically and plotted in the same figure. The mean first-passage time $H(i, j)$ is defined as the average time for the classical random walker to visit node j for the first time, starting the walk from node i. We can interpret $H(\mathrm{hub}, w)$ as the average time to search the marked node by starting the classical random walk from the hub node. From Fig. 6(a), we can confirm that the time it takes to search a node using the random walk is proportional to its degree [32], as well as revealing that the search using the quantum walk clearly shows a different feature.

Figure 6(b) shows the case of eigenvector centrality $C_w^e = |\langle\lambda_1|w\rangle|$, which is a centrality measure based on the leading eigenvector of the adjacency matrix. The plot shows a high correlation as expected from Eq. (8). We also see a good correlation in Fig. 6(c), which shows the case of closeness centrality $C_w^c = (N-1)/\sum_{j\neq w}^{N-1} l_{wj}$, where l_{wj} is the shortest path distance between nodes w and j. This measure represents how fast one can move from the node w to all other nodes using the shortest paths.

TABLE II. Exponent α of the average search time $T \propto N^{\alpha}$ for nodes with different distances from the hub $l_{\mathrm{hub},w}$. Networks with parameters $N = 2000$–$10\,000$, $m = 5$, $\beta = 3$ are used to obtain α.

$l_{\mathrm{hub},w}$	1	2	3
α	0.120 ± 0.019	0.638 ± 0.122	1.127 ± 0.205

Figure 6(d) shows the betweenness centrality $C_w^b = \sum_{i \neq w \neq j} \sigma_{ij}(w)/\sigma_{ij}$, where σ_{ij} is the number of shortest paths from node i to j, and $\sigma_{ij}(w)$ is the number of shortest paths that goes through node w among them. The random-walk closeness centrality $C_w^{\mathrm{rc}} = N/\sum_j H(j,w)$ in Fig. 6(e) is an alternative measure of the closeness centrality, where path lengths between nodes are measured based on the random-walk process. The random-walk betweenness centrality C_w^{rb} in Fig. 6(f) is an alternative measure of betweenness centrality, where instead of counting only the shortest paths, all paths contribute to the measure with a certain weight. All three of these measures are correlated with the search time in a similar way to the degree centrality.

The results presented in Fig. 6 tell us that the quantum walk or the spatial search is a dynamic relying on the shortest paths of the network, unlike the classical random walk. In the case of the classical random walk, the walker chooses one neighbor randomly at each time step, and thus it is natural to understand that a node having a larger degree will have a higher probability to receive the walker, leading to a shorter time of the search. In contrast, since the quantum walker spreads to all of the neighbors as a superposition state, the length of the shortest paths between the nodes determines the time for the complex amplitudes to reach from one node to another, rather than the degrees. As indicated by the high correlation to the closeness centrality C_w^c, if the marked node w is averagely close to all other nodes (i.e., if it has high C_w^c), the quantum walker can localize on that node faster since the complex amplitudes of the quantum walker can be collected from the whole network with a shorter time.

The importance of the distances is emphasized by distinguishing the data points in Fig. 6 based on the shortest path distance between the hub node and the marked node (see the legend of the figure). The data are well clustered depending on $l_{\mathrm{hub},w}$. Especially when the marked node is adjacent to the hub ($l_{\mathrm{hub},w} = 1$), these nodes have small shortest-path distances with the other nodes by going through the hub, leading to the shortness of T.

We also examined how the scaling of the search time $T \propto N^{\alpha}$ depends on the distance between the hub and the marked node $l_{\mathrm{hub},w}$. We computed multiple samples of T_w from the networks with parameters $N = 2000$–$10\,000$, $m = 5$, $\beta = 3$ and we took the average of T_w for each $l_{\mathrm{hub},w}$. The obtained scaling α is shown in Table II. Although we get large standard deviations of T_w since the factor determining the search time is not only $l_{\mathrm{hub},w}$, the scaling α roughly increases linearly as $l_{\mathrm{hub},w}$ grows.

Note that the especially short T when the marked node is adjacent to the hub is not due to the localized initial state of the quantum walker. The quantum walker does not instantaneously hop from the hub to the marked node, but instead has to traverse the entire network and acquire some phase to localize on the marked node. In fact, from Eq. (8) we can see that the optimal evolution time $\tau = \pi/\Delta E$ is independent of the initial state. The initial state determines the fraction of the complex amplitude that stays in the two-dimensional subspace spanned by $|E_0\rangle$ and $|E_1\rangle$, and thus only affects the maximum success probability $P(\tau)$.

Although the high correlation between the search time and the eigenvector centrality is expected from Eq. (8), there are small corrections from the factor $|\langle w|\tilde{w}\rangle|$, which is essentially the success probability P. In our results, we did not see a particularly high correlation between the centrality measures and P. The best correlation we could observe was with the eigenvector centrality, with correlation coefficient $r = 0.363$.

V. DISCUSSIONS

In this paper, we have analyzed the performance of the continuous-time spatial search algorithm on the Bollobás model, which is a scale-free network. We found that the search time is faster as the marked node is more central in the network, where this is measured by the closeness centrality of the node. Such a feature results from the power-law degree distribution and the existence of the large-degree hub node of the scale-free network. Interestingly, the degree of the marked node does not crucially matter for the search time, but the shortest path distances between the marked node and the rest of the nodes determine the search time. We can interpret that the search time is dependent on how fast the marked node can collect the complex amplitudes globally from the network (and thus the global structure matters). This is in contrast to searching by a classical random walk, which is highly dependent on how many edges are locally connected to the marked node. We also observed that the distribution of the search time in a network follows a multimode log-normal distribution, which reflects well the structure of the scale-free network. We characterized the interesting relationship between the network structure and the performance of the spatial search algorithm, which could not have been discovered using regular or homogeneous graphs.

The localized property of the leading eigenvector of the adjacency matrix was advantageous in a way that we could select an initial state that was fully localized on a single node, instead of a superposition state. We can generally say that if the search Hamiltonian Eq. (3) without the $\epsilon_w|w\rangle\langle w|$ term has a localized ground state, one can choose a localized initial state. This may be advantageous in experimental implementations, since preparing a superposition state with arbitrary amplitudes and relative phases can be difficult [36]. However, such a localized leading eigenvector also creates differences in the optimal measurement time τ depending on the marked node. This fundamentally limits the ability to perform the spatial search algorithm, since we need some amount of information about the node that is searched for in order to estimate the measurement time. However, as the distribution of the search time is well separated into classes depending on whether the node is adjacent to the hub, one can make a reasonable guess of τ by limiting the nodes to be marked within one class. In addition, we can naturally translate the dynamics of the spatial search algorithm into

an efficient state transfer protocol between the hub node and a single marked node [25,49], which is a simple and useful application.

ACKNOWLEDGMENTS

We thank Benjamin Renoust for helpful discussions. This project was made possible through the support of a grant from the John Templeton Foundation, Grant No. ID 60478. The opinions expressed in this publication are those of the authors and do not necessarily reflect the views of the John Templeton Foundation. This work was also supported in part by the MEXT Quantum Leap Flagship Program (MEXT Q-LEAP) Grant No. JPMXS0118069605. B.C. and Y.O. thank the support from Fundação para a Ciência e a Tecnologia (Portugal), namely through programme POCH and projects UID/EEA/50008/2019 and UIDB/50008/2020, as well as from projects TheBlinQC and QuantHEP supported by the EU H2020 QuantERA ERA-NET Cofund in Quantum Technologies and by FCT (QuantERA/0001/2017 and QuantERA/0001/2019, respectively), and from the EU H2020 Quantum Flagship project QMiCS (820505)

[1] R. Albert and A. L. Barabási, Rev. Mod. Phys. **74**, 47 (2002).
[2] S. N. Dorogovtsev, A. V. Goltsev, and J. F. F. Mendes, Rev. Mod. Phys. **80**, 1275 (2008).
[3] M. E. J. Newman, in *Proceedings of the National Academy of Sciences*, edited by B. Skyrms (University of California Press, Irvine, CA, 2006), Vol. 103, p. 8577.
[4] A. L. Barabási and R. Albert, Science **286**, 509 (1999).
[5] N. Pržulj, Bioinformatics **23**, 177 (2007).
[6] S. Boccaletti, V. Latora, Y. Moreno, M. Chavez, and D. U. Hwang, Phys. Rep. **424**, 175 (2006).
[7] M. E. J. Newman, Phys. Rev. E **66**, 016128 (2002).
[8] Y. Moreno, M. Nekovee, and A. F. Pacheco, Phys. Rev. E **69**, 066130 (2004).
[9] R. Pastor-Satorras, C. Castellano, P. Van Mieghem, and A. Vespignani, Rev. Mod. Phys. **87**, 925 (2015).
[10] J. Smith, A. Lee, P. Richerme, B. Neyenhuis, P. W. Hess, P. Hauke, M. Heyl, D. A. Huse, and C. Monroe, Nat. Phys. **12**, 907 (2016).
[11] D. N. Biggerstaff, R. Heilmann, A. A. Zecevik, M. Gräfe, M. A. Broome, A. Fedrizzi, S. Nolte, A. Szameit, A. G. White, and I. Kassal, Nat. Commun. **7**, 11282 (2016).
[12] L. Schlipf, T. Oeckinghaus, K. Xu, D. B. R. Dasari, A. Zappe, F. F. D. Oliveira, B. Kern, M. Azarkh, M. Drescher, M. Ternes, K. Kern, J. Wrachtrup, and A. Finkler, Sci. Adv. **3**, e1701116 (2017).
[13] V. M. Bastidas, B. Renoust, K. Nemoto, and W. J. Munro, Phys. Rev. B **98**, 224307 (2018).
[14] M. Faccin, P. Migdał, T. H. Johnson, V. Bergholm, and J. D. Biamonte, Phys. Rev. X **4**, 041012 (2014).
[15] G. Bianconi, Europhys. Lett. **111**, 56001 (2015).
[16] J. Biamonte, M. Faccin, and M. D. Domenico, Commun. Phys. **2**, 53 (2019).
[17] M. Pant, H. Krovi, D. Towsley, L. Tassiulas, L. Jiang, P. Basu, D. Englund, and S. Guha, npj Quantum Inf. **5**, 25 (2019).
[18] P. Benioff, in *Quantum Computation and Information*, AMS Contemporary Mathematics Series, edited by S. J. Lomonaco and H. E. Brandt (AMS, Washington, D.C., 2002).
[19] S. Aaronson and A. Ambainis, in *44th IEEE Symposium on Foundations of Computer Science, Cambridge, MA* (IEEE, Piscataway, NJ, 2003), p. 200.
[20] A. M. Childs and J. Goldstone, Phys. Rev. A **70**, 022314 (2004).
[21] A. M. Childs and Y. Ge, Phys. Rev. A **89**, 052337 (2014).
[22] I. Foulger, S. Gnutzmann, and G. Tanner, Phys. Rev. Lett. **112**, 070504 (2014).
[23] J. Janmark, D. A. Meyer, and T. G. Wong, Phys. Rev. Lett. **112**, 210502 (2014).
[24] L. Novo, S. Chakraborty, M. Mohseni, H. Neven, and Y. Omar, Sci. Rep. **5**, 13304 (2015).
[25] S. Chakraborty, L. Novo, A. Ambainis, and Y. Omar, Phys. Rev. Lett. **116**, 100501 (2016).
[26] S. Chakraborty, L. Novo, and J. Roland, arXiv:1807.05957.
[27] E. Agliari, A. Blumen, and O. Mülken, Phys. Rev. A **82**, 012305 (2010).
[28] S. D. Berry and J. B. Wang, Phys. Rev. A **82**, 042333 (2010).
[29] P. Philipp, L. Tarrataca, and S. Boettcher, Phys. Rev. A **93**, 032305 (2016).
[30] B. Bollobás and O. M. Riordan, Combinatorica **24**, 5 (2004).
[31] B. Bollobás, in *Handbook of Graphs and Networks, 2003*, edited by S. Bornholdt and H. G. Schuster (Wiley-VCH, Weinheim, 2003), p. 1.
[32] J. D. Noh and H. Rieger, Phys. Rev. Lett. **92**, 118701 (2004).
[33] E. M. Bollt and D. ben-Avraham, New J. Phys. **7**, 26 (2005).
[34] Z. Zhang, Y. Qi, S. Zhou, W. Xie, and J. Guan, Phys. Rev. E **79**, 021127 (2009).
[35] A. Glos, R. Kukulski, A. Krawiec, and Z. Puchal, Quantum Inf. Proc. **17**, 81 (2018).
[36] C. Godfrin, A. Ferhat, R. Ballou, S. Klyatskaya, M. Ruben, W. Wernsdorfer, and F. Balestro, Phys. Rev. Lett. **119**, 187702 (2017).
[37] S. N. Dorogovtsev, J. F. F. Mendes, and A. N. Samukhin, Phys. Rev. Lett. **85**, 4633 (2000).
[38] G. Caldarelli, A. Capocci, P. De Los Rios, and M. A. Muñoz, Phys. Rev. Lett. **89**, 258702 (2002).
[39] E. Ravasz and A. L. Barabási, Phys. Rev. E **67**, 026112 (2003).
[40] Ch. Dangalchev, Physica A **338**, 659 (2004).
[41] D. Krioukov, F. Papadopoulos, M. Kitsak, A. Vahdat, and M. Boguna, Phys. Rev. E **82**, 036106 (2010).
[42] C. Song, S. Havlin, and H. A. Makse, Nat. Phys. **2**, 275 (2006).
[43] K. I. Goh, B. Kahng, and D. Kim, Phys. Rev. E **64**, 051903 (2001).
[44] P. F. Bonacich, Amer. J. Sociol. **92**, 1170 (1987).
[45] L. C. Freeman, Social Netw. **1**, 215 (1979).
[46] L. C. Freeman, Sociometry **40**, 35 (1977).
[47] S. White and P. Smyth, in *Proceedings of the Ninth ACM SIGKDD International Conference on Knowledge Discovery and Data Mining, Washington, D.C.* (ACM, New York, NY, 2003), p. 266.
[48] M. E. J. Newman, Social Netw. **27**, 39 (2005).
[49] M. Štefaňák and S. Skoupý, Phys. Rev. A **94**, 022301 (2016).